Appendix: Development of Expression for Approximate Ignition Time

The physical basis of approximate ignition time for the semi-infinite solid with DPL conduction takes advantage of the expected behavior for its surface temperature: For small values of time after the application of q_0 along the surface $x = 0$, internal heating by reaction should be small compared with external heating by q_0 because the surface temperature and associated reaction rate are still relatively low. Thus, these small time values correspond to a period of nearly inert (nonreactive) heating dominated by q_0. During this inert period, the surface temperature is approximated by the solution to the corresponding inert DPL problem where $S = 0$. For large times, however, the surface temperature is high enough for heating by reaction to dominate and cause thermal runaway. Hence, approximate ignition time t^* is defined here as that intermediate time when rates of internal heating by reaction and external heating by q_0 become momentarily equal. The surface temperature at t^* is the corresponding approximate ignition temperature T^*.

Reference 2 develops an expression for approximate ignition time by using the physical basis of t^* just described but for hyperbolic conduction. (Reference 2 terms this hyperbolic approximation the "rough approximation.") Thus, by analogy, developing the expression for t^* with DPL conduction starts with Eq. (1A) in Ref. 2 because that equation is a convenient form for T^* of the semi-infinite solid regardless of the model chosen for conduction. Then T^* is eventually related to t^* for DPL conduction. Consequently, introducing β, δ, γ, and dimensionless DPL approximate ignition temperature φ^* into Eq. (1A) of Ref. 2 and then solving for φ^* gives

$$\varphi^* = (1/\gamma)[\beta/\ell n(\delta/2\gamma) - 1] \tag{A1}$$

Equation (A1) here arises from the equivalence of external and internal heating underlying the approximate ignition time.

Completing the development for DPL conduction requires obtaining a relation between φ^* and ξ^* and then using this relation to replace φ^* by ξ^* in Eq. (A1). For this relation to be obtained, Eq. (1) from the main body of this Note is first made dimensionless by using B, φ, β, δ, and γ, along with η and ξ. In particular, $\eta = 0$ is the surface of the semi-infinite solid where ignition occurs at ξ^*. This dimensionless form of Eq. (1) replaces Eq. (3A) in Ref. 2. Next, with the use of the same reasoning as in Ref. 2, the dimensionless form of Eq. (1), with appropriate boundary and initial conditions, reduces to that describing the problem for the DPL inert heating period. Section 3.1 in Ref. 6 states this inert problem, with some differences in nomenclature from that of this Note. The solution to this inert problem for $B < \frac{1}{2}$ is given by Eq. (12) in Ref. 6. Converting that equation to the nomenclature of this Note and then setting $\eta = 0$ and $\xi = \xi^*$ in the converted equation provides the relation between φ^* and ξ^*. Then using this relation to replace φ^* in Eq. (A1) here provides the implicit expression for ξ^* when $B < \frac{1}{2}$, given as Eq. (2) in the main body of this Note. Alternatively, the expression for ξ^* when $B \geq \frac{1}{2}$ is obtained by using Eq. (11) from Ref. 6 in place of Eq. (12).

References

[1] Tzou, D. Y., *Macro- to Microscale Heat Transfer: The Lagging Behavior*, Taylor and Francis, Washington, DC, 1997, pp. 124, 147–166.

[2] Antaki, P. J., "Importance of NonFourier Heat Conduction in Solid Phase Reactions," *Combustion and Flame*, Vol. 112, No. 3, 1998, pp. 329–341.

[3] Nakazawa, K., Asako, Y., Jin, Z. F., and Yamaguchi, Y., "Transient Thermal Responses in Glass Beads Packed Bed," *Proceedings of the National Heat Transfer Conference*, Vol. 12, American Society of Mechanical Engineers, New York, 1997, pp. 169–174.

[4] Varma, A., and Lebrat, J. P., "Combustion Synthesis of Advanced Materials," *Chemical Engineering Science*, Vol. 47, No. 9–11, 1992, pp. 2179–2194.

[5] Lebon, G., Torrisi, M., and Valenti, A., "A Non-Local Thermodynamic Analysis of Second Sound Propagation in Crystalline Dielectrics," *Journal of Physics: Condensed Matter*, Vol. 7, No. 7, 1995, pp. 1461–1474.

[6] Antaki, P. J., "Solution for Non-Fourier Dual Phase Lag Heat Conduction in a Semi-Infinite Slab with Surface Heat Flux," *International Journal of Heat and Mass Transfer*, Vol. 41, No. 14, 1998, pp. 2253–2258.

Band Lumping Strategy for Radiation Heat Transfer Calculations Using a Narrowband Model

Fengshan Liu,* Gregory J. Smallwood,† and Ömer L. Gülder‡

National Research Council, Ottawa, Ontario K1A 0R6, Canada

Nomenclature

f	= species molar fraction or the distribution function of the absorption coefficient
g	= cumulative distribution function
g_i	= the ith Gauss quadrature point
I_i	= radiation intensity at the ith quadrature point, W/m^2 cm^{-1} sr
k	= absorption coefficient, m^{-1}
k_i	= absorption coefficient at the ith quadrature point, m^{-1}
L	= path length, m
s	= position variables along a line of sight, m
T	= temperature, K
w_i	= weight parameter of the ith Gauss quadrature point
$\Delta\nu$	= wave number interval of a band, cm^{-1}
ν	= wave number, cm^{-1}
$\bar{\tau}$	= band-averaged gas transmissivity

Subscripts

b	= blackbody
nb	= narrowband
wb	= wideband

I. Introduction

ACCURATE calculations of real-gas radiation are inherently difficult due to the extremely strong spectral variations of gas radiative properties. In combustion, real-gas practically means CO_2 and H_2O present in the combustion products for hydrocarbon fuels. Oversimplified gas radiation models yield large errors in the prediction of gas radiation and cannot be used as a reliable radiation submodel in an overall combustion or flame code. The exact line-by-line (LBL) calculations, however, are far too computationally intensive to be applied to problems of practical interest. Therefore, substantial research efforts have been devoted to development of accurate and efficient nongrey gas radiation models.

The statistical narrowband correlated-k (SNBCK) method represents an efficient alternative for implementing the statistical narrowband (SNB) model. The method has recently been applied to two-dimensional real-gas radiation transfer by Goutière et al.,[1] and they found that the SNBCK method yields total quantities almost identical to those of the SNB model with far less computing effort. The SNBCK method overcomes the difficulties of the SNB model because it extracts gas absorption coefficients from the SNB gas transmissivity. As a result, any radiative transfer equation (RTE) solvers, especially the efficient and accurate discrete-ordinates method (DOM), can be used. Extension of the SNBCK method to scattering problems is straightforward. The seven-point

Received 7 May 1999; revision received 20 October 1999; accepted for publication 10 November 1999.

*Associate Research Officer, Institute for Chemical Process and Environmental Technology, Combustion Research Group, Montreal Road. Member AIAA.

†Senior Research Officer, Institute for Chemical Process and Environmental Technology, Combustion Research Group, Montreal Road.

‡Group Leader, Institute for Chemical Process and Environmental Technology, Combustion Research Group, Montreal Road.

Gauss–Lobatto quadrature has been commonly employed in various correlated-k (CK) and narrowband weighted-sum-of-gray-gases methods.[2–4]

In the present study, a band lumping strategy was developed to formulate a wideband CK model within the context of the SNBCK method. The strategy can be applied to other narrowband CK methods. Band lumping groups several (typically 5–20) successive narrowbands into a wideband and calculates the radiative transfer over the wideband, instead of solving the RTE several times at each narrowband inside the wideband. In general, the more narrowbands lumped, the more efficiency is gained, at the cost of larger errors because the blackbody function cannot be treated as constant as the bandwidth increases. Numerical calculations were conducted using the SNBCK method with and without band lumping, and the results were compared with those of the SNB model.

II. Band Lumping Strategy

The SNBCK method has been described in detail previously by Lacis and Oinas[5] and Goody et al.[6] and recently by Liu et al.[7,8] The SNB model parameters employed in the present study are those presented by Soufiani and Taine.[4] Because the bandwidth is uniform at 25 cm^{-1} in this SNB model database, the mean gas transmissivity over a wideband containing M successive narrowbands is calculated as

$$\bar{\tau}_{wb} = \frac{1}{M}\sum_{i=1}^{M} \bar{\tau}_i \tag{1}$$

where $\bar{\tau}_i$ is the mean gas transmissivity of the ith narrowband inside the wideband and is calculated according to the SNB model. For narrowbands of nonequal width, the wideband gas transmissivity is then the bandwidth weighted average, instead of the simple algebraic average, of the gas transmissivities of narrowbands inside the wideband. The inverse Laplace transformation of Eq. (1) yields the absorption coefficient distribution function at the wideband:

$$f_{wb}(k) = \frac{1}{M}\sum_{i=1}^{M} f_i(k) \tag{2}$$

where the normalized distribution function at each narrowband $f_i(k)$ is given in the SNBCK method. By definition, the cumulative distribution function at the wideband is calculated similarly:

$$g_{wb}(k) = \frac{1}{M}\sum_{i=1}^{M} g_i(k) \tag{3}$$

Inversion of the preceding equation yields the gas absorption coefficients at the wideband, which can be done efficiently using a Newton–Raphson iteration method described by Lacis and Oinas[5] and Liu et al.[7,8] Note that an equation similar to Eq. (3) has been presented by Marin and Buckius[9] based on a different argument and for a different purpose.

When the resultant wideband contains overlapping narrowbands of CO_2 and H_2O, the band lumping strategy described is first applied to each radiating gas component then the effect of band overlapping is handled using the correlated treatment discussed by Lacis and Oinas[5] and Liu et al.[7]

III. Results and Discussion

To demonstrate the accuracy and efficiency of the SNBCK method with and without band lumping for radiation transfer over widebands and over the entire infrared, numerical calculations were carried out for band-integrated intensities along a line of sight and radiation heat transfer in a one-dimensional, parallel-plates enclosure. Results from the SNB model were used as the reference solution in the comparisons. For calculations using the SNB model, the correlated transfer equation discussed by Kim et al.[10] was solved. The seven-point Gauss–Lobatto quadrature given in Ref. 2 was used in all of the SNBCK calculations. Whenever band lumping was employed, the blackbody intensity was assumed constant over the wideband and evaluated at the center of the wideband. The pressure of the radiating gas is assumed at 1 atm throughout this work. All of the calculations were performed on an SGI Octane workstation at 175 MHz.

The integral form of the RTE was solved. Spectrally integrated quantities are calculated by adding the appropriate band quantities (wall heat fluxes and volumetric source term) over all of the bands.

Band-Integrated Intensities Along a Line of Sight

Numerical calculations were performed for three levels of band lumping for three gas columns having different concentration and temperature distributions. The length of the three gas columns considered is $L = 1$ m between $x = 0$ and 1 m. The left wall at $x = 0$ is assumed black and cold at 300 K. Band-integrated intensities at $x = 1$ m and along the positive x direction were calculated. The gas in column 1 is a homogeneous H_2O–N_2 mixture with $f_{H_2O} = 0.2$, and the temperature is uniform at 1800 K. The gas in column 2 is a homogeneous CO_2–N_2 mixture with $f_{CO_2} = 0.1$, and the temperature is also uniform at 1800 K. Column 3 contains a nonisothermal and inhomogeneous CO_2–H_2O–N_2 mixture with $T = 1000 + 1400 \times 4 \times x/L - 1400 \times 4 \times (x/L)^2$, $f_{CO_2} = 0.05 + 0.1 \times 4 \times x/L - 0.1 \times 4 \times (x/L)^2$, and $f_{H_2O} = 0.6 - 0.4 \times 4 \times x/L + 0.4 \times 4 \times (x/L)^2$. A uniform grid of 80 was used in the calculations.

Figure 1 shows the band-integrated intensities calculated using the SNBCK method with and without band lumping for columns 1 and 2. In Fig. 1, SNBCK7-1band denotes results obtained using the seven-point Gauss–Lobatto quadrature and without band lumping, that is, summation of intensity of each narrowband inside the wideband, whereas SNBCK7-$n$band ($n > 1$) represents results based on lumping n narrowbands. Results of the SNB model are not shown because they are almost identical with those of the SNBCK7-1band. For column 1, results of 5- and 10-band lumping are in excellent agreement with those without band lumping (Figs. 1a and 1b). Although the results of 20-band lumping show slight deviation from the unlumped results at bands centered below 2000 cm^{-1}, the agreement is still very good. This deviation is expected because the blackbody function varies quite sharply at 1800 K at low wave numbers, and it is no longer constant over a bandwidth of 500 cm^{-1} (20 narrowband lumping). For column 2, results of 5- and 10-band lumping are in good agreement with those without band lumping, with small errors present at bands near 2200 cm^{-1} (Figs. 1a and 1b). Results of

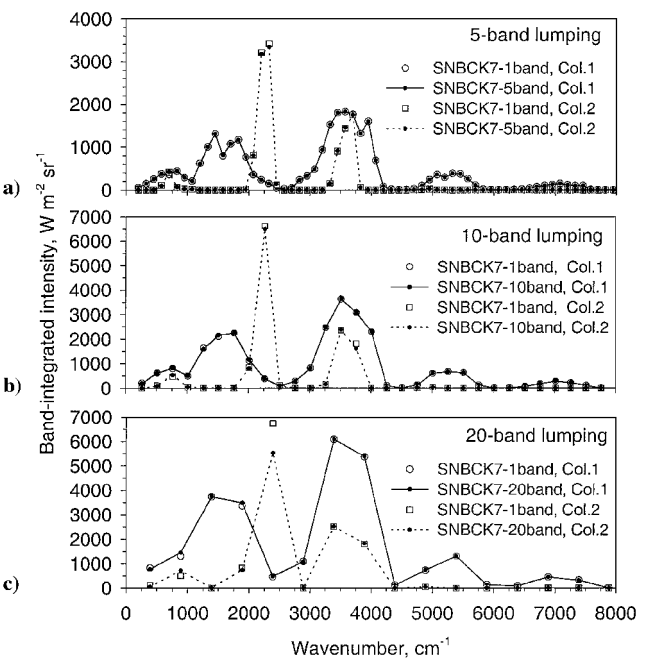

Fig. 1 Comparisons of band-integrated intensities calculated using the SNBCK method with and without band lumping for columns 1 and 2: a) 125 cm^{-1} bandwidth, b) 250 cm^{-1}, and c) 500 cm^{-1}.

Table 1 CPU times of the SNBCK method for calculations of the one-dimensional case

Method	CPU, s
SNBCK7-1band	328
SNBCK7-5band	81
SNBCK7-10band	52
SNBCK7-20band	41

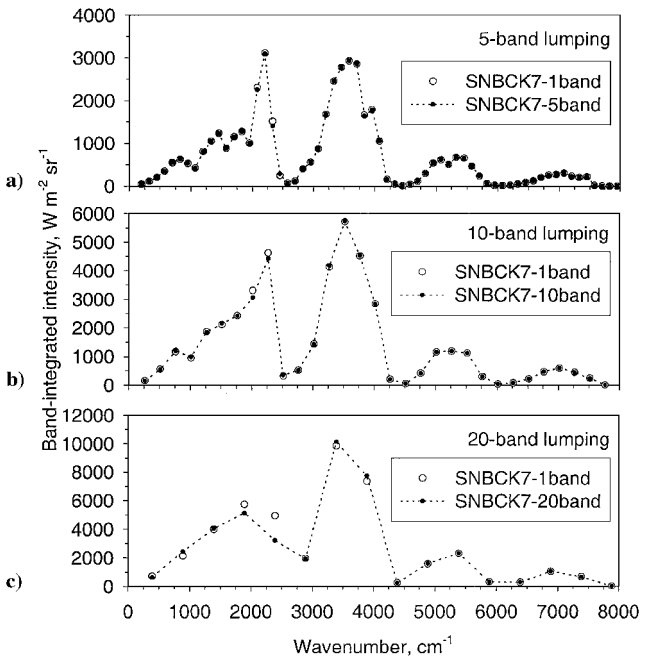

Fig. 2 Comparisons of band-integrated intensities calculated using the SNBCK method with and without band lumping for column 3: a) 125 cm^{-1} bandwidth, b) 250 cm^{-1}, and c) 500 cm^{-1}.

20-band lumping are still in good agreement with the unlumped results, except at the 2387.5 cm^{-1} band, where the lumped intensity is about 18% lower (Fig. 1c). This large discrepancy shown in Fig. 1c for column 2 at 2387.5 cm^{-1} is attributed to the strong radiating and extremely banded behavior of the 4.3-μm band of CO_2. It is possible to improve the accuracy of the band lumping results near the 4.3-μm band of CO_2 by optimizing the bandwidth and band locations of lumped bands, instead of using uniform bandwidth.

Results of column 3 are shown in Fig. 2. For this nonisothermal inhomogeneous case, results with band lumping still display good agreement with those without band lumping, especially for 5- and 10-band lumping. Errors in the band lumping results increase as the number of narrowbands lumped increases due to the greater variation of the blackbody intensity over a wider spectral interval. It is interesting, but not too surprising, to see that errors of results with band lumping are greatest near bands around 2200 cm^{-1} at all three levels of band lumping, especially for 20-band lumping (Fig. 2c). This is caused by the 4.3-μm band of CO_2 based on the results of column 2 shown in Fig. 1.

Spectrally Integrated Quantities in a One-Dimensional, Parallel-Plates Enclosure

Spectrally integrated quantities were calculated in a one-dimensional, parallel-plates enclosure. The separation distance between the two plates is 1 m, and the conditions of the mixture bounded by the two plates are the same as those in column 3. The two bounding surfaces are black and at 0 K. Numerical calculations were conducted using 40 uniform grids and the T_4 angular quadrature (containing 128 directions in the entire 4π solid angle). The CPU times of different runs using the SNBCK method with and without band lumping are compared in Table 1.

The CPU time ratio of the SNBCK7-1band to the SNBCK7-10band is only about 6.3. Apparently, there is an unexpected behavior of band lumping because one might expect that such a ratio should be close to 10. However, a thorough study of the CPU time consumption of the SNBCK calculations provides the explanation for this unexpected result. In the SNBCK calculations using a N point quadrature at each narrowband, that is, no band lumping, it is found that most of the CPU time is spent on inversion of $g(k)$ and the RTE solver, that is,

$$t_{\text{nb}} = Nt_{\text{inversion}} + Nt_{\text{solver}} \tag{4}$$

where t_{nb}, $t_{\text{inversion}}$, and t_{solver} are the CPU times spent on each narrowband calculation, on $g(k)$ inversion, and on RTE solver at each quadrature point, respectively. Therefore, the CPU time spent on calculations of a wideband containing M narrowbands is

$$t_{\text{wb, no lumping}} = MNt_{\text{inversion}} + MNt_{\text{solver}} \tag{5}$$

When radiative transfer over a wideband is calculated using the band lumping strategy, the CPU time is found approximately to be

$$t_{\text{wb, with lumping}} = MNt_{\text{inversion}} + Nt_{\text{solver}} \tag{6}$$

The last two equations indicate that band lumping saves CPU time on the RTE solver, but not on $g(k)$ inversion. This can be understood by the formulation of the cumulative distribution function at a wideband given in Eq. (3), which contains time-consuming exponential operations.[5,7] This is why the CPU time reduction does not scale linearly with the number of narrowbands lumped. Table 1 shows that the CPU time saving decreases as the number of narrowbands lumped increases.

The source term distributions (not shown) calculated using SNBCK7-1band, SNBCK7-5band, and SNBCK7-10band are almost identical with the SNB results, indicating that 5- or 10-band lumping causes negligible errors in radiation heat transfer calculations. Errors of the results based on 20-band lumping are still very small, only about 2% compared to those of SNB. The wall heat flux densities calculated using the SNBCK method with and without band lumping are in very good agreement with the SNB result. The SNBCK7-20band lumping run gave rise to the largest error of about only 3%.

IV. Conclusions

A band lumping strategy was developed to calculate radiative transfer over a wideband or the entire infrared using the SNBCK method in CO_2, H_2O, and their mixtures to improve the efficiency of the SNBCK method for such applications. Based on the numerical results obtained in this study, the following conclusions are reached.

1) The band lumping strategy yields accurate results with about 20 narrowbands of 25 cm^{-1} lumping for radiative transfer in CO_2–H_2O–N_2 mixtures even under non-isothermal and inhomogeneous conditions. The more narrowbands are lumped, the less accurate the results are. Most of the errors of band lumping results may be attributed to the nonoptimized partition of the 4.3-μm band of CO_2 rather than the variation of the blackbody intensity over a bandwidth of about 500 cm^{-1}.

2) The CPU time saving of the SNBCK method with the band lumping strategy does not scale linearly with the number of narrowbands lumped. The CPU time saving decreases as the number of narrowbands lumped increases.

3) A 10 narrowband lumping is recommended based on considerations of accuracy and efficiency.

References

[1]Goutière, V., Liu, F., and Charette, A., "An Assessment of Real Gas Modelling in 2D Enclosures," *Journal of Quantitative Spectroscopy and Radiative Transfer*, Vol. 64, No. 3, 2000, pp. 299–326 .

[2]Rivière, P. H., Soufiani, A., and Taine, J., "Correlated-*k* and Fictitious Gas Methods for H_2O Near 2.7 μm," *Journal of Quantitative Spectroscopy and Radiative Transfer*, Vol. 48, No. 2, 1992, pp. 187–203.

[3]Yang, S.-S., and Song, T.-H., "An Improved WSGGM-Based Narrow-Band Model for the CO_2 4.3 μm Band," *International Journal of Thermal Science*, Vol. 38, No. 3, 1999, pp. 228–238.

[4]Soufiani, A., and Taine, J., "High Temperature Gas Radiative Property Parameters of Statistical Narrow-Band Model for H_2O, CO_2 and CO, and Correlated-K Model for H_2O and CO_2," *International Journal of Heat and Mass Transfer*, Vol. 40, No. 4, 1997, pp. 987–991.

[5]Lacis, A. A., and Oinas, V., "A Description of the Correlated k Distribution Method for Modeling Nongray Gaseous Absorption, Thermal Emission, and Multiple Scattering in Vertically Inhomogeneous Atmosphere," *Journal of Geophysical Research*, Vol. 96, No. D5, 1991, pp. 9027–9063.

[6]Goody, R., West, R., Chen, L., and Crisp, D., "The Correlated-k Method for Radiation Calculations in Nonhomogeneous Atmospheres," *Journal of Quantitative Spectroscopy and Radiative Transfer*, Vol. 42, No. 6, 1989, pp. 539–550.

[7]Liu, F., Smallwood, G. J., and Gülder, Ö. L., "Application of the Statistical Narrow-Band Correlated-k Method to Non-Grey Gas Radiation in CO_2–H_2O Mixtures: Approximate Treatments of Overlapping Bands," *Journal of Quantitative Spectroscopy and Radiative Transfer* (submitted for publication).

[8]Liu, F., Smallwood, G. J., and Gülder, Ö. L., "Application of the Statistical Narrow-Band Correlated-k Method to Low-Resolution Spectral Intensity and Radiative Heat Transfer Calculations—Effects of the Quadrature Scheme," *International Journal of Heat and Mass Transfer* (to be published).

[9]Marin, O., and Buckius, R. O., "A Model of the Cumulative Distribution Function for Wide Band Radiative Properties," *Journal of Quantitative Spectroscopy and Radiative Transfer*, Vol. 59, No. 6, 1998, pp. 671–685.

[10]Kim, T.-K., Menart, J. A., and Lee, H. S., "Nongray Radiative Gas Analysis Using the S-N Discrete Ordinates Method," *Journal of Heat Transfer*, Vol. 113, No. 4, 1991, pp. 946–952.

Non-Fourier Heat-Flux Law for Diatomic Gases

Abdulmuhsen H. Ali*
Kuwait University, Safat 13060, Kuwait

Nomenclature

$E^{\text{int}}(v, r)$ = internal energy of the reduced mass
$E^{\text{kin}}(v)$ = kinetic part of the internal energy
$E^{\text{pot}}(r)$ = potential part of the internal energy
$E^{\text{tr}}(V)$ = translational energy of the center of mass
$E(V, v, r)$ = total energy, $E^{\text{tr}}(V) + E^{\text{int}}(v, r)$
$\{\hat{e}_l\}$ = set of linearly independent basis
$f^{(1)}(\boldsymbol{R}, \boldsymbol{V}, t)$ = local equilibrium distribution function for the center of mass:

$$n_M(\boldsymbol{R}, t)[M\beta(\boldsymbol{R}, t)/2\pi]^{\frac{3}{2}} \times \exp\{-[M\beta(\boldsymbol{R}, t)/2][\boldsymbol{V} - \boldsymbol{u}_M(\boldsymbol{R}, t)]^2\}$$

$f^{(1)}(\boldsymbol{R}, \boldsymbol{v}, t)$ = local equilibrium distribution function for the reduced mass:

$$n_\mu(\boldsymbol{R}, t)[\mu\beta(\boldsymbol{R}, t)/2\pi]^{\frac{3}{2}} \times \exp\{-[\mu\beta(\boldsymbol{R}, t)/2][\boldsymbol{v} - \boldsymbol{u}_\mu(\boldsymbol{R}, t)]^2\}$$

$g(|\boldsymbol{r}|)$ = radial or pair distribution function, $\exp[\beta W(r)]$
$\boldsymbol{J}(t)$ = heat flux
k_B = Boltzmann constant
M = total mass of the diatomic molecule
$n_M(\boldsymbol{R}, t)$ = number density of the total mass
$n_\mu(\boldsymbol{R}, t)$ = number density of the reduced mass
$\hat{n}$ = unit vector
q = real number
$\boldsymbol{R}$ = position vector of the center of mass
$\boldsymbol{r}$ = position vector of the relative distance between two point particles
r_m = distance between point particles at which their potential energy is minimum
T = temperature
t = time
$\boldsymbol{u}_M(\boldsymbol{R}, t)$ = center-of-mass average velocity vector, $\langle \boldsymbol{V} \rangle$
$\boldsymbol{u}_\mu(\boldsymbol{R}, t)$ = reduced-mass average velocity vector, $\langle \boldsymbol{v} \rangle$
$\boldsymbol{V}$ = velocity of the center of mass
$\boldsymbol{v}$ = velocity of the relative position vector between two point particles
$W(r)$ = potential energy of the average force a particle experiences
β = $1/k_B T$
β^*_{dia} = Eucken number for diatomic gases:

$$\left[\beta^*_{\text{tr}} - \frac{(5 - 3\gamma)}{3(\gamma - 1)}\beta^*_{\text{int}}\right]$$

β^*_{int} = Eucken number caused by internal states:

$$3\left[1 - \frac{\mu(\delta v)^2}{3k_B T} + \frac{2\langle E^{\text{int}} W(r)\rangle}{3\langle E^{\text{int}}\rangle k_B T}\right]$$

β^*_{tr} = Eucken number caused by translational motion, $3[1 - M(\delta V)^2/3k_B T]$
Γ = arbitrary volume over which the relative coordinate is integrated
γ = ratio of heat capacities
Δ = variable's nonequilibrium instantaneous departure from its equilibrium value
$\Delta \boldsymbol{a}$ = total area:

$$\int_{\text{open surface}} \mathrm{d}\boldsymbol{a}$$

δ = fluctuation in a variable
∂_t = derivative with respect to time, $\partial/\partial t$
ϵ = perturbation
θ = time as an integration variable
λ = thermal conductivity of diatomic gases, $\beta^*_{\text{dia}}\langle E^{\text{tr}}\rangle u/2T\Delta a$
λ_{int} = thermal conductivity caused by internal motion, $\beta^*_{\text{int}}\langle E^{\text{int}}\rangle u/2T\Delta a$
λ_{tr} = thermal conductivity caused by translational motion, $\beta^*_{\text{tr}}\langle E^{\text{tr}}\rangle u/2T\Delta a$
μ = reduced mass of the diatomic molecule
σ = physical constant, $\beta^*_{\text{dia}}\langle E^{\text{tr}}\rangle/3\Delta a$
τ = relaxation time
$\langle\ \rangle$ = nonequilibrium ensemble average
$\langle\ \rangle_e$ = equilibrium ensemble average

Introduction

PREVIOUSLY a derivation of the Cattaneo's heat-flux law, which is a non-Fourier heat-flux law, was given for monoatomic gases.[1] The derivation of Cattaneo's heat-flux equation for diatomic gases will emphasize the validity of the method used before for monoatomic gases, which is an important thing to do before the method is applied to the far-from-equlibrium case, and will demonstrate the phenomenon of finite speed heat propagation for a different kind of gas, namely the diatomic gas. Therefore, the derivation of Cattaneo's heat-flux equation for diatomic gases is presented here. Under special conditions, which include being at the critical temperature, the method used before proved very successful here in the case of diatomic gases. However, the distribution function that

Received 10 September 1999; revision received 16 November 1999; accepted for publication 16 November 1999.

*Assistant Professor, Department of Physics, P.O. Box 5969; alie@kuc01.kuniv.edu.kw.